Deducing Flow Path Mixing by Storm-Induced Bulk Chemistry and REE Variations in Two Karst Springs: With Trends Like These Who Needs Anomalies?

Corresponding author: James L. Berglund, Department of Earth and Environmental Science, Temple University, Philadelphia, PA, USA, 19122, james.berglund@temple.edu

Laura Toran, Department of Earth and Environmental Science, Temple University, Philadelphia, PA, USA, 19122, ltoran@temple.edu

Ellen K. Herman, Department of Geology, Bucknell University, Lewisburg, PA, USA, 17837, ekh008@bucknell.edu

Citation: Berglund, J.L. Toran, L., and Herman, E.K. In press. Deducing Flow Path Mixing by Storm-Induced Bulk Chemistry and REE Variations in Two Karst Springs: With Trends Like These Who Needs Anomalies? Accepted in Journal of Hydrology, January 2019.

Key words: karst; karst spring; rare earth elements; storm hydrograph; flow mixing; Valley and Ridge Province

Abstract

Karst aquifers are dynamic hydrologic systems which can be sensitive to short-term recharge events (storms) and heterogeneous recharge characteristics (point recharge at sinks, irregular soil thicknesses). In this study, two adjacent karst springs, Tippery Spring and Near Tippery Spring, were monitored to better understand flow and source mixing characteristics in response to two storms in May and June 2017. Monitoring techniques included high-resolution discharge and temperature logging and collection of spring water using automatic samplers to analyze chemical parameters such as stable water isotopes and Mg/Ca ratios along with Ca/Zr ratios and rare earth elements (REEs) which have had limited testing in karst systems. The two springs exhibited behaviors which were both unique to each spring and shared depending on which parameter is considered. Spring-specific behaviors included discharge and isotopic response, with Tippery Spring having a flashier and faster conduit flow behavior relative to Near Tippery Spring's delayed storm response. Absolute Mg/Ca values were spring-specific, owing to the relative fraction of limestone and dolostone in their respective recharge areas, although both springs showed similar Mg/Ca ratio shifts after storms. While Ca/Zr ratios changed in timing and intensity with storm intensity, both springs exhibited a decline in Ca/Zr ratios as calcium-rich carbonate matrix water was displaced by zirconium-rich storm recharge water from sinking streams off the clastic upland ridges. Flushing of recharged storm water resulted in an increase in total REE concentrations at both springs (from <0.15 ppb to >1.0 ppb), with the timing and magnitude of concentration increases determined by the degree of surface connectivity intrinsic to each spring and the intensity of the recharge event. REEs and Ca/Zr ratios provided additional and complementary tracer techniques to better understand transient recharge and flow behaviors in karst springs.

1. Background

1.1 Assessing Transient Behaviors in Karst

As conduits make karst aquifers particularly vulnerable to contamination from a variety of sources, quantifying the proportion of conduit flow is essential to aquifer protection. The karst aquifer network and clastic sediments within serve not only as transmission pathways for contaminants, but also as long- and short-term storage reservoirs for contaminants. Numerous approaches exist to characterize the structure and behavior of karst aquifers to address the inherent uncertainties in these complex hydrologic systems (Thrailkill, 1987; Mangin, 1994; Padilla, A. et al., 1994; Larocque et al., 1998; Pinault et al., 2001; White, 2002; Bakalowicz, 2005; Goldscheider, 2015; Scanlon, B.R.). These approaches have included correlations between surficial karst features and flow (Kresic, 1995), hydrological modeling approaches (Hill, 2010), dye tracing (Goldscheider, 2008), geophysical methods (Schwartz and Schreiber, 2009), and spring monitoring (Desmarais and Rojstaczer, 2002). Temperature and specific conductance are

easily measured with relatively inexpensive, easily deployable data loggers, allowing for the collection of high-frequency data sets over long periods of time. Monitoring physiochemical parameters of spring water, both seasonally and in response to storm events, is an especially useful means to understanding karst aquifer behaviors. Short term and seasonal variations in spring water chemistry can provide insight into source water mixing and ground water residence times feeding a spring. As such many attempts have been made to characterize karst springs based on their discharge and physiochemical parameters. One of the earlier spring classifications by Shuster and White (1971) used temperature and major ion chemistry to classify springs as conduit-flow dominant and matrix-flow dominant.

More recent studies have further sought to classify and characterize other elements of flow behavior, such as vadose vs. phreatic storage using stable water isotopic analysis (Lakey and Krothe, 1996), fast-flow and slow-flow components based on discharge recession curves (Doctor, 2005), localized vs. distributed recharge based on spring temperature patterns (Luhmann, 2011), and conduit-flow vs. matrix-flow components based on Mg/Ca ratios during storm flow (Toran and Reisch, 2013). Goldscheider (2015) pointed out the need for multiple tracers such as dyes to determine fast flow paths and natural tracers such as stable water isotopes for slow flow paths. Lack of variation in isotope signals during storm events has been used as evidence of mixing of fast and slow paths not indicated by other tracers (Winston and Criss, 2004; Schwarz et al., 2009). Thicker soil cover leading to slower recharge has been used to explain some isotope mixing (Zhao et al., 2018). The lag between discharge response and conductivity response has been used to estimate travel times (Birk et al., 2004). Seasonal variation in mixing along flow paths has been demonstrated by discriminant factor analysis of major ions and Mg/Ca ratio in a study by Bicalho and others (2012). Chloride and specific conductance have been used to evaluate variations in contributions such as activation of deeper flow paths (Ravbar et al., 2011; Martin et al., 2016).

While these approaches allowed for improved conceptual models of karst aquifers, critical knowledge gaps still remain regarding recharge and flow paths within a karst system. We classify karst flow systems to better understand the complex pathways formed by the fast flow paths in conduits and slow flow paths through the matrix. In actuality, the matrix comprises both primary and fracture porosity and permeability, resulting in a flow system that is a continuum from larger to smaller openings and from conduit to diffuse flow. Thus, the discharge chemistry reflects output from varied recharge, fast flow paths, slow flow paths, and flow paths that result from mixing of conduit and matrix water. To move beyond using end members to describe flow paths, it is important to evaluate multiple storm events and use multiple tracers to capture these variations.

1.2 Rare Earth Elements as Natural Tracers

Rare earth elements (REEs) show potential for determining recharge zones and flow paths in karst aquifers. REEs are a group of elements comprising the lanthanide series (lanthanum (La), cerium (Ce), praseodymium (Pr), neodymium (Nd), promethium (Pm), samarium (Sm),

europium (Eu), gadolinium (Gd), terbium (Tb), dysprosium (Dy), holmium (Ho), erbium (Er), thulium (Tm), ytterbium (Yb), and lutetium (Lu)) plus scandium (Sc) and yttrium (Y)) (Henderson, 1984). The main chemical difference throughout the lanthanide series is the progressive shrinking in ionic radius from 115 pm (La) to 93 pm (Lu) which imparts distinct behaviors in their fractionation and incorporation into minerals (White, 2015). Due to the similar ionic radii between neighboring REEs, they tend to maintain similar relative abundances in nature despite significantly variable absolute abundances. With the exception of cerium, which can have a +2 valence, and europium, which can have a +4 valence, the REEs have a +3 valence. The variable valence state for cerium and europium allows them to fractionate relative to their neighbors under certain environmental conditions, such as redox variations, making them useful natural geochemical tracers (Leybourne and Johannesson, 2008).

REE patterns from host materials can also be transferred to water, providing a useful tool for tracing recharge areas and flow paths (Playà et al., 2007). Hydrological studies have used REEs to better understand flow paths through water-rock interactions (Johannesson et al., 1997; Tang and Johannesson, 2006; Göb et al.,, 2013), recharge conditions (Möller et al., 2006; Tweed et al., 2006; Willis and Johannesson, 2011), and transport (Ingri, 2000; Pourret, 2010).

In an early study, Johannesson et al. (1997) observed the unique REE patterns of carbonate and felsic rocks were imparted in waters recharging through them, allowing for groundwater mixing to be assessed between the two sources further along in their flow paths. Möller et al. (2006) also noted the imparting of lithological REE patterns on groundwater in a region with variable basalt, basalt-limestone, limestone, and gypsum dominated recharge areas. Willis and Johannesson (2011) observed homogeneous flat shale-normalized REE patterns and groundwater compositions throughout an aquifer indicating relatively homogeneous recharge patterns through shale-weathered bulk sediments. Ingri et al. (2000) reported on the positive relationship between REE concentrations and sediment weathering, with a strong linear correlation being noted between REE concentrations and dissolved aluminum (Al) derived from Al-rich sediments. Other authors, such as Tang and Johannesson (2006), measured dissolved REE concentrations throughout a sand aquifer, which generally decreased in concentration, indicating changes in redox and pH conditions along flow paths. Tweed et al. (2006) explored changing REE patterns along an aquifer's flow paths, noting increased REE concentrations when pH conditions were lowest (<6.1) typically near the aquifer's recharge area, with decreasing REE concentrations as pH increased downgradient. Studies on the mobility of REEs, such as by Pourret et al. (2010), have noted the tendency for REEs to be sorbed and strongly mobilized with colloids. In addition to variable concentrations, Göb et al. (2013) reported on the presence of negative cerium (Ce) anomalies in oxidized waters due the variable oxidation states of Ce controlling its mobility.

Studies exploring REE transport and temporal variability, though, are still limited (Ingri et al., 2000; Pourret et al., 2010; Gill, 2018). Additionally, the relative significance and complexity of the factors controlling REE patterns in hydrologic systems, such as redox, pH, colloidal transport, and host rock contribution, are still not entirely understood (Noack et al., 2014; Duvert, 2015).

The application of REEs to better understand flow paths and recharge makes them promising tools in karst aquifers which are inherently complex. Johannesson and others (2000) observed that shale-normalized REE patterns in aquifer water reflected that of the host rock, with carbonate rocks exhibiting heavy REE enrichment and negative Ce anomalies. Gill and others (2018) used contrasting REE ratios (e.g., Pr/Yb, Y/Ho) between limestone and sandstone in a lowland karst network to determine varying recharge contributions from each lithology. Zhou and others (2012) identified middle rare earth element (MREE) enrichment in stalagmites related to changing recharge conditions through the overlying soil layer. Toran and others (2018) used REEs to identify springs with a greater contribution to discharge from slow flow through the carbonate bedrock matrix. Subdued REE signatures were observed after rain events in karst springs (Filippini et al., 2018). Despite these results, more research is needed, especially into behaviors unique to karst systems such as temporal variability and recharge heterogeneity.

For this study, the two adjacent springs were analyzed for natural tracers. These tracers can provide a more complete understanding of source area, recharge, and flow behavior feeding the two springs.

2. Study Site

Two karst springs, Tippery and Near Tippery, were chosen for storm response monitoring (Figure 1). These springs have been included in historic and recent research for examining the similarities and differences in their recharge and flow behaviors. Their separate yet adjacent capture areas provide identical rainfall conditions since the springs are only 65 m apart, but allow for comparison of recharge and flow path differences. Located within the folded and faulted Valley and Ridge Province of central Pennsylvania's Nittany Valley, the two springs emerge from the foot of Canoe Mountain, a topographic ridge which merges with Brush Mountain and Bald Eagle Mountain to the west which form the western boundary of the Allegheny Front (Berg et al., 1980). Canoe Mountain forms the axis of a syncline with Silurian and Ordovician sandstones forming the ridges and Ordovician shales and carbonates forming the flank and foot of the ridge, respectively. Minor streams off the ridge typically flow after storms, although some streams, such as Tippery Sink, are perennial. These streams often feed sinkholes in the carbonate rocks, which in turn feed nearby springs. Tippery Spring has been traced to three upland sinkholes, while Near Tippery Spring has been traced to one sinkhole, with no observed cross-over between capture areas (Hull, 1980). Dye trace travel times were less than 48 hours for Tippery Spring and less than 72 hours for Near Tippery Spring. Both springs show similar baseflow discharges of 0.14-0.28 m^3/sec with storm flow discharges up to 0.85 m^3/sec (Shuster and White, 1971). The drainage area of each spring is estimated to be around 3-4 km^2, extending up to the ridgetop (Herman et al., 2009; Hull, 1980). The springs are at an elevation of 274 meters MSL, with a capture area extending up to the ridge top of 396 meters. Both springs have variable discharge, temperature, and chemistry at the seasonal scale (Shuster and White, 1971) and storm-response scale (Herman et al., 2009).

A study by Berglund and others (2018) re-examined Tippery Spring and Near Tippery Spring from the Shuster and White (1971) study by comparing stable water isotope chemistry after storm recharge. The results revealed recharge behaviors which were dependent on both the size

of the storm and the intrinsic recharge characteristics of each spring. For a given storm size, Tippery Spring showed a flashier storm hydrograph response than Near Tippery Spring, which translated into a relatively greater portion of storm water based on stable water isotopes. In contrast, Near Tippery Spring had a buffered stable water isotope response, showing a lesser overall portion of storm water, spread across the hydrograph. Along with high-resolution data, these results allowed for a greater understanding of the two springs' recharge and flow behaviors.

3. Methods

3.1 Spring Monitoring

Water temperature and pressure were recorded at 15-minute intervals using Onset HOBO pressure loggers. Rectangular weirs with openings measuring 100 cm wide and 34 cm tall at each spring allowed water level to be converted to discharge. Water pH was recorded using Manta2 data loggers at 15-minute intervals. During field visits pH data were collected using an IQ Scientific Instruments IQ150 meter with a Thermo Scientific Orion 9106BNWP pH electrode to provide calibration and drift correction. Specific conductance (SC) was measured after sample retrieval using an Extech Instruments 407313 conductivity and temperature meter. Total suspended solids (TSS) was calculated from weighing 0.45 μm filter paper before and after filtration. A HOBO rain gauge logger recorded rainfall on-site. A 7-day antecedent precipitation index (API), which is an index of soil moisture from recent rainfall weighted towards more recent rain events, was calculated for each storm (Ali et al., 2010):

$$API = \sum_{t=-1}^{-i} P_t k^{-1} \quad (1)$$

where API = antecedent precipitation index (cm); P_t = rainfall (cm) that occurs from time t; t = time (days); k = recession constant from 0.8-0.98 (0.9 used for this study, a typical value used in the cited literature). A larger API indicates more recent and intense storm events, while a lower API indicates a drier period.

3.2 Sample Collection

Water samples were collected during two storm events; a 2.5 cm storm in May 2017 (Figure 2) and a 7.6 cm storm in June 2017 (Figure 3). ISCO 3700 auto-samplers containing 24, 1-liter, acid-washed bottles, collected spring water samples triggered by rising spring water level in response to each storm. The 24 samples at each spring were collected over the course of 24 hours with a higher initial sampling rate (every 30 minutes) then progressively slower frequency (to every 2 hours) to capture more variable initial geochemical signatures. ISCO bottles were recovered within 1-3 days after the storm. When possible, grab samples were also collected before and after the storm. All water samples were filtered with 0.45 μm nitrocellulose paper and refrigerated in headspace-free bottles until analysis. As water samples were filtered with 0.45 μm filters, elemental analysis of water samples does not differentiate among relative contribution of different physical components (truly dissolved, small particulate, and colloidal) smaller than 0.45 μm.

Samples analyzed for rare earth elements, cations, and heavy metals were acidified with ultra-high purity nitric acid after filtering.

3.3 Sample Analysis

Major ion analysis was performed using a Thermo Scientific iCAP 7200 inductively coupled plasma optical emission spectrometry (ICP-OES) analyzer and a Dionex ion chromatography (IC) analyzer. Alkalinity was measured with a Hanna Instruments HI 775 alkalinity colorimeter. Stable isotope analysis ($^{18}O/^{16}O$ and D/H) was performed using a Laser Water Isotope Analyzer V2 (Los Gatos Research Inc., UC Davis Isotope Laboratory, Mountain View, CA) and reported relative to Vienna Standard Mean Ocean Water (VSMOW). Water samples were analyzed for rare earth element concentrations using inductively coupled plasma mass spectrometry (ISO/IEC 17025 Accredited ICP-MS, Geoscience Laboratories, Ontario Geological Survey, Sudbury, Ontario, Canada). Rare earth element concentrations were normalized to the Post-Archean Australian Shale (PAAS) for spidergram and anomaly analysis (Pourmand et al., 2012). The cerium anomaly (Ce*) is the ratio of the normalized Ce concentration to the expected value from interpolation between the measured values of La and Pr (Noack, 2014).

$$Ce^* = \frac{2*[Ce]}{La + Pr} \quad (2)$$

4. Results

4.1 Monitored Storms

The May 2017 Storm began on May 4, 2017, at 19:00 EST; precipitation lasted for 13 hours, with a total rainfall of 2.54 cm. Two days prior to the May 2017 Storm event, a slight drizzle (1.25 cm) fell on the study site. As such, slightly wet antecedent conditions prevailed at the onset of the sampling event (7-day API = 2.94). The water sampling period continued until 16:30 EST on May 6, 2017. Due to the wet antecedent conditions, discharges at Tippery Spring and Near Tippery Spring were slightly elevated above their average annual base flow values (0.03 m^3/s and 0.01 m^3/s, respectively) to 0.11 m^3/s and 0.09 m^3/s, respectively. In response to the storm, Tippery Spring reached a peak flow of 0.86 m^3/s fourteen hours after the start of rainfall and receded to 0.49 m^3/s by the end of sampling. Near Tippery Spring reached a peak flow of 0.46 m^3/s fifteen hours after the start of rainfall with a variable discharge plateau (0.37-0.49 m^3/s) for the remainder of the sampling period.

The June 2017 Storm fell during two pulses; the first beginning on June 15, 2017, at 19:00 EST and depositing 5.30 cm of rain over 7 hours, and the second beginning on June 16, 2017, at 16:00 EST depositing 2.30 cm of rain over 2 hours. Spring water sampling continued until 1:30 EST on June 17. Little to no rainfall occurred prior to the June 2017 Storm (7-day API = 0.06). Due to the dry antecedent conditions, discharges at Tippery Spring and Near Tippery Spring initially had their annual average base flow values of 0.03 m^3/s and 0.01 m^3/s, respectively. In response to the storm, Tippery Spring reached a peak flow of 1.20 m^3/s seven hours after the onset of rainfall, and recovered to 0.23 m^3/s twelve hours later, then peaked again at 1.19 m^3/s three hours after the beginning of the second period of rainfall, and recovered slightly to 0.95 m^3/s by the

end of the sampling period. Near Tippery Spring reached a peak flow of 0.59 m^3/s seven hours after the first occurrence of rainfall, recovered to 0.39 m^3/s ten hours later, then peaked again at 0.61 m^3/s six hours after the second onset of rainfall. Near Tippery recovered slightly to 0.53 m^3/s by the end of the sampling period.

4.2 Storm Chemographs

4.2.1 Parameter groupings

Water level (calibrated to discharge at a weir), temperature, and pH were measured using dataloggers which provided high-resolution and easily retrievable indicators of storm water arrival at the springs. Total suspended solids (TSS), specific conductance (SC), alkalinity, calcite saturation index (SI_C), and stable water isotopes (δ^2H & $\delta^{18}O$) were analyzed from water samples as they provide information on spring chemistry changes during storm flow, such as matrix water dilution, carbonate rock dissolution and saturation, and parsing of isotopically distinct pre-storm water and storm water fractions. In addition, this study examined the temporal variations in molar Mg/Ca ratios and Ca/Zr ratios, and metals such as Fe and Zr, and REEs. Mg/Ca ratios indicate varying conduit-matrix water interactions as matrix water tends to have higher Mg/Ca ratios than conduit water. Metals were analyzed to further explore their relationship with REE mobility and concentration. Zr was selected as a potential indicator of upland source waters as Zr concentrations in the upland sandstones and shales are found in higher concentrations than in the local carbonate rocks from whole rock analysis (131 ppm and 16 ppm, respectively), as similarly noted by Hua and others (2013). Ca/Zr ratios were explored as an indicator of recharged storm water from the clastic upland ridges which are enriched in Zr and depleted in Ca relative to the carbonate bedrock. Both δ^2H & $\delta^{18}O$ fell linearly along the local meteoric water line, so only δ^2H is shown in chemographs. For each spring, chemographs were produced from continuous loggers and samples from automatic sampling, along with grab samples during post-storm baseflow conditions (Figures 4-7).

Certain parameters varied together in the chemographs for both springs, and there were different patterns for the parameter groups. Being carbonate springs with high Ca concentrations, the chemical parameters SC, alkalinity, and SI_C tended to vary together, with the Mg/Ca ratio showing similar variability but a slightly more complex response. Stable water isotopes and Ca/Zr ratios also showed similar timing to these chemical parameters in the initial response, but differed later in the hydrograph. TSS, metals, total REEs, and the Ce anomaly grouped together based on their similar timing, suggesting transport with or as sediment for these constituents. Temperature and pH varied from storm to storm and did not show similar timing to the other variables. Temperature sometimes showed a storm pulse, although long-term temperature logger data showed that not all storm events have a temperature signal (Toran et al., 2018). Little change in temperature was observed during the May Storm at either spring due to the relatively small size of the storm and lack of temperature contrast between the storm water and ambient ground water. In contrast, the June Storm resulted in a notable temperature change at both springs due to a greater amount of rainfall and a greater temperature contrast between storm water and ambient ground water, producing a temperature spike for each storm pulse at Tippery Spring and a gradual increase at Near Tippery Spring.

4.2.2 Pre-storm conditions

Pre-storm conditions varied for both springs before the two storms. May pre-storm concentrations were likely a consequence of the wet antecedent conditions prior to the May Storm (Figure 4 for Tippery and Figure 6 for Near Tippery). This included elevated TSS and dissolved metals (Fe, Zr), slightly enriched stable isotope values, decreased SC, alkalinity, Ca/Zr ratio, and calcite SI. The pre-storm water chemistry prior to the June Storm was more typical of baseflow samples for both springs during this study and from previous historical sampling (Shuster and White, 1971). In addition, the initial Mg/Ca ratio differed between the two springs for both storms. Tippery Spring's pre-storm water chemistry parameters showed low Mg/Ca ratios, reflecting the predominantly limestone flow path area, while Near Tippery Spring had a higher overall Mg/Ca ratio due to the relatively greater fraction of dolomite within its flow path (Figure 1).

4.2.3 Tippery Spring chemographs

At Tippery Spring during both storms, a brief (approximately 1-hour) spike in pH, SC, alkalinity, and SI_C signaled the initial arrival of storm water; this increase was likely flushing of older, more concentrated water stored in the system (Figures 4 and 5). This spike occurred just before the stable isotope signal of storm water, indicated by rising δ^2H partway through the rising limb of the discharge hydrograph. The Mg/Ca ratio also spiked although slightly delayed from the other initial responses. As the storm water isotope signal arrived, SC and alkalinity became diluted followed by a gradual recovery for the May Storm (Figure 4). For the June Storm, the same initial dilution from arriving storm water was observed, but the larger storm resulted in a slightly longer dilution period and more gradual recovery that was interrupted by a second storm event (Figure 5). The Mg/Ca ratio followed these trends with slight differences. During the May Storm the dilution period for Mg/Ca was slightly longer than for SC and other dissolved constituents, and the recovery was slower as well. The timing of the Mg/Ca ratio also differed from other dissolved constituents in the June Storm: there was a larger initial increase (possibly piston flow component of older water) and a delay in the dilution phase. The second storm water pulse during the June Storm produced a second increase in Mg/Ca. The Ca/Zr ratio and the stable water isotope signature followed inverse trends. Ca/Zr decreased along with other chemical parameters as the δ^2H increased. However, these two parameters showed a slower recovery compared to the other dissolved constituents.

The arrival of the storm pulse at Tippery Spring was accompanied by an increase in TSS, trace metals (shown by Fe and Zr) and total REEs. This increase began at the same time as the isotope storm water increase, but peaked slightly later then showed an asymmetrical long tail decline that lingered longer than other dissolved constituents. The Ce anomaly followed a similar pattern but returned to pre-storm baseflow values sooner than the total REEs and metals (Figures 4 and 5).

4.2.4 Near Tippery Spring chemographs

Near Tippery showed a similar grouping of dissolved constituent response and sediment parameter response, but with slightly different timing (Figures 6 and 7). The initial storm signal arrived later in the discharge hydrograph, after the peak for both the May and the June Storms. There was no initial spike as observed at Tippery in several parameters. However, for the June Storm, a signal from additional overland flow was observed initially. This overland flow was triggered by the larger June Storm and was indicated by a rapid storm signal (increase in storm water stable isotopes, temperature, and sediment, along with dilution of dissolved constituents). The overland flow mixing with spring flow has been observed for large storms during site visits. The separate arrival of groundwater storm discharge at Near Tippery Spring was indicated by a decrease in the dissolved constituents (SC, alkalinity, SI_C, Ca/Zr ratio, and Mg/Ca ratio) and an increase in the stable water isotope signature. During the May Storm, dilution in the dissolved constituents was followed by a rebound to concentrations above the baseflow conditions (except for Ca/Zr), then a gradual decline back to baseflow levels on the falling limb of the hydrograph. During the June Storm, recovery did not rebound to concentrations above the baseflow conditions. The timing of the changes in Mg/Ca ratio for the May Storm was similar to the other parameters. However, for the June Storm the Mg/Ca ratio responded faster relative to the other parameters, and a rise in Mg/Ca was seen for the second storm pulse in June. The Ca/Zr ratio and the isotope signature both showed a slower recovery to baseflow values than other chemical parameters. For both storms, the sediment associated parameters (TSS, Fe, Zr, and REEs) showed the same pattern at Tippery Spring and Near Tippery Spring, with an increase on the rising limb and an asymmetrical decrease on the falling limb.

4.2.5 Comparison of storm responses

The timing and degree of response varied based on the size of the storm event (the larger June Storm vs. the weaker May Storm) and the intrinsic nature of recharge of each spring's capture area (Tippery Spring having a larger storm water recharge volume compared to Near Tippery Spring) as indicated by stable isotopes (Berglund et al., 2018).

The dilution and recovery was more gradual at Near Tippery Spring than at Tippery Spring and more gradual for the larger June Storm compared to the smaller May Storm. The TSS, metal, and REE concentrations also increase later at Near Tippery Spring than at Tippery Spring, and recovered more gradually than the chemical parameters at both springs.

4.3 Spring REE Spidergrams during Storm Response

With the exception of europium, all individual REE concentrations were above detection limits, albeit at low concentrations. PAAS-normalized plots of individual REE concentrations for a single water sample (called spidergrams) illustrated internal REE trends and anomalies resulting from geochemical processes and water-rock interactions in the May Storm where pre- and post-storm samples were available for clear comparison with baseflow water chemistry (Figures 8 and 9). Only the May Storm was selected here due to the availability of pre- and post-storm samples

to make inferences about lingering effects of storms on REE characteristics. Baseflow sampling of select carbonate springs in Pennsylvania (including Tippery Spring and Near Tippery Spring) for cerium anomalies suggested that springs with a greater component of slow matrix flow contain more prominent negative cerium anomalies (Ce*<1) (Toran et al., 2018). This relationship was further explored here where relative contributions of faster conduit flow and slower matrix flow varied in response to storm recharge.

For Tippery Spring (Figure 8), REE patterns during pre-storm flow had low REE concentrations with a slightly negative cerium anomaly. There was also a non-detect of europium (time A). The apparent europium anomaly during baseflow conditions is the result of being near or below detection limit instead of association with the carbonate bedrock, and its behavior is not considered further here. At peak REE concentrations (time B) there were no cerium anomalies. As REE concentrations began to drop to pre-storm levels (time C) the slightly negative cerium anomaly returned. At the time where other spring chemistry parameters recovered (time D), REE concentrations were still slightly elevated above their pre-storm values. Despite other indicators of slow matrix flow contributions flow contribution, a strong cerium anomaly was not seen at Tippery Spring during any period of storm response. This further highlights Tippery Spring's greater conduit-flow influence, even during baseflow, but also suggests that a cerium anomaly may be a sensitive indicator of conduit flow mixing with slow matrix flow during storm recovery.

For Near Tippery Spring (Figure 9), REE patterns during pre-storm flow (time A') were similar to Tippery Spring, having low overall REE concentrations and non-detect of europium, but differed by having a notably negative cerium anomaly. This cerium anomaly discrepancy between the two springs was also observed in the baseflow sampling (Toran et al., 2018). During peak REE concentrations in response to storm flow (time B') the cerium anomaly was eliminated. A slight return of the cerium anomaly was observed during the REE concentration recovery (time C'). REE concentrations remained slightly elevated with the return of the cerium anomaly (time D') after other chemical parameters have recovered.

The presence of the negative cerium anomaly during baseflow suggests carbonate bedrock interaction and its subsequent anomaly neutralization during storm flow suggests faster flow paths. Storm water REEs had similar REE patterns to the PAAS shale standard, with no enrichment in light, middle or heavy REEs (LREE/MREE/HREE), but instead showed a relatively flat pattern. The lack of anomalies, and similar REE pattern to the PAAS shale standard further support that stormflow REE enrichment is sourced in the detrital clastics upgradient feeding into the carbonate sinkholes rather than in the carbonate rocks themselves.

5. Discussion

The two springs shared a similar cycle of storm response characterized by three distinct periods (Figure 10). The three periods are similar for each storm, but nonetheless there are distinctions between the two springs. There were differences in arrival times of storm pulses for the two

springs and longer recovery times for the larger storm. The differences between these three periods provide evidence for mixing along their recharge and flow paths.

Period 1: Piston Flow: Spring discharge rises shortly after rainfall due to a piston flow effect from increased pressure head in the recharge area. No geochemical variation in spring mouth chemistry occurred at Near Tippery Spring during this period, while a short spike in chemical parameters occurred at Tippery Spring indicating purging of older, more concentrated pre-storm water, which has been observed in other karst springs (Birk et al., 2004; Ravbar et al., 2011; Ryan and Meiman, 1996). The purging of older water and faster flow response at Tippery Spring are indicative of faster flow paths. In contrast, Near Tippery's discharge showed mixing between source waters derived from both fast and slow flow responses.

Period 2: Arrival of storm water from a combination of faster and slower flow-dominated recharge: This period begins with the arrival of fast-flow storm water through conduits connected to surface runoff from the ridge tops. This storm water pulse was indicated by signatures such as an enrichment in stable water isotope values and dilution of chemical parameters, including Ca/Zr. The dilute storm water was then replaced by water from slower flow paths signaled by an increase in SC, alkalinity, SI_C and Mg/Ca ratio. Mixing of waters from fast and slow flow paths was observed, however, based on different patterns in the timing of chemical parameters. In previous studies, mixing induced by storms has been observed by Cl^- fluctuation in the chemograph (Mitrofan et al., 2015), by age dating (Martin et al., 2016), by isotope tracers (Schwarz et al., 2009), and by variation in temperature and SC particularly at low flow periods (Filippini et al., 2018).

The timing of period 2 differs between Tippery Spring and Near Tippery Spring. Tippery Spring showed storm water on the rising limb of the hydrograph. For Near Tippery Spring, period 2 begins 4-6 hours after the peak flow plateau is reached, with storm water gradually rising to a maximum about 12 hours after peak flow. This slower response is likely due to Near Tippery Spring's decreased conduit-flow portion in discharge, creating a flow buffering capacity.

The slightly different timing in Mg/Ca ratios at both springs compared to the other chemical parameters suggested that mixing can be complex. As Mg/Ca increases, more contact with the matrix is inferred, while faster flow paths are inferred from Mg/Ca decreases. There were both increases and decreases in the Mg/Ca ratio observed in period 2. We detailed the Mg/Ca ratio because it is an important example of mixing. As conduits vary from larger to smaller openings, varying degrees of interaction occur with the matrix. Furthermore, different recharge events can capture from varying areas, also creating variable mixtures. Thus, at Near Tippery Spring during the May Storm, the Mg/Ca ratio declined at a similar time as SC and other dissolved constituents, but showed an earlier decline than SC in the June Storm. At Tippery Spring, Mg/Ca ratios took longer to recover than SC and other chemical parameters for the May Storm. For the June Storm, Mg/Ca increased while SC decreased, indicating a stronger matrix component possibly indicating a piston flow pulse of older water. This piston flow component may explain the delayed dilute storm water signature in Mg/Ca ratios. Thus, period 2 showed both increases and decreases in Mg/Ca ratios at Tippery Spring which provided evidence of mixing of fast and slow flow paths.

All parameters showed a more extended storm signal and recovery for the larger June Storm, as expected. The June Storm resulted in about two times more discharge than the May Storm at Tippery Spring and nearly three times more discharge at Near Tippery Spring. The dilution factors and recovery periods differed more between the May and June storms at Near Tippery, even though the flow is the more buffered at this spring. The contrast in discharge between the two storms and larger dilution reflects the slower travel times to Near Tippery Spring. Mg/Ca ratios varied more than SC and other dissolved constituents. Thus, each spring has storm-to-storm differences in response indicating that flow paths include varied portions of conduit and slow components depending on the storm. A more buffered spring may require longer sampling periods to capture chemograph variations and faster flow paths require finer time intervals.

Recharge source area parameters also appear during this period, such as an increase in TSS, which signaled flushing of surface sediments, and the decrease in Ca/Zr ratios, which indicated the arrival of waters interacting with Zr-rich and Ca-poor ridgetop sediments feeding sinks and sinkholes. Parameters associated with sediments such as REEs and metals also increased during this period. This study pointed out that ion ratios can better indicate chemical variations that tag source areas (Ca/Zr) and matrix components (Mg/Ca).

Period 3: Recovery to new base flow fed by slower matrix-dominated flow paths: The third period was marked by a decline in TSS and metals for the May Storm. There was more TSS variation in the June Storm, and recovery was interrupted by a second storm, so a distinct period 3 was not observed at either spring. The length of time for recovery was difficult to estimate with the gap between automated sampler measurements and the second storm event in June, although for a given rainfall event Tippery Spring showed a shorter recovery time than Near Tippery Spring.

For both storms, the REE concentrations retained a storm pulse signal (i.e., slightly elevated concentration) longer than TSS and chemical parameters in the recovery period. Spring discharge also remained elevated as the water chemistry returned to concentrations similar to pre-storm periods (high Mg/Ca, SI_C closer to saturation). In addition to the high discharge, the stable water isotopes and Ca/Zr ratio were slow to recover to pre-storm conditions. The long tail of recovery for these components provides further evidence of mixing of flow paths and storm water input that extends further than indicated by the dilution and recovery of dissolved constituents such as SC.

In summary, although these periods in the hydrographs and chemographs of karst springs have been identified in previous studies (e.g., Ford and Williams, 2007; Ravbar et al., 2011), the analysis here pointed out additional complexity in the arrival of storm water in period 2. By examining multiple tracers these mixing patterns were identified as well as storm-to-storm variations. The importance of continuous monitoring, including the tail of the hydrograph was also reinforced by the monitoring at these adjacent springs. Variations in age and mixing in springs that are in close proximity have been identified previously, particularly at low flow (Martin et al., 2016; Filippini et al., 2018), but the distances were on the order of kilometers. In this study the springs were only 65 m apart and still showed distinct responses in the storm chemographs.

5.2 Ca/Zr ratios as indicators of storm recharge source area

One relationship which stood out during storm water arrival was the ratio between Ca and Zr in relation to stable water isotope storm water fraction. Comparing Ca/Zr ratios to storm water fraction determined from stable water isotopes (Berglund et al., 2018) showed a mixing relationship between pre-storm water with a high Ca/Zr ratio, and a storm water component with low Ca/Zr (Figure 11). Prior to the influence of storm recharge, base flow matrix water contained elevated Ca relative to Zr, as the carbonate bedrock contains little detrital Zr contributing to stored water. During storm flow, a drop in Ca/Zr ratio corresponded to the arrival of storm water as indicated from the stable water isotopes. This ratio decrease during the arrival of storm water was due to the concurrent decrease of Ca concentration and increase in Zr concentration. The decrease in Ca concentration was due to the flushing and dilution of high-Ca matrix water by recharging storm water, which contains little to no Ca. In contrast, Zr concentrations increased with increasing storm water component. This increased Zr concentration likely resulted from storm water having interacted with surficial clastic sediments with elevated concentrations of Zr relative to the carbonates. These clastic sediments are transported after storms by the sinking streams draining the clastic ridge tops which feed into sinkholes within the carbonate rock at the foot of the hills. As a result, Ca/Zr ratios provided both a useful indicator of storm water arrival along with source of recharge water. As the analyzed water samples included materials below 0.45 μm, Ca and Zr are transported in both dissolved and colloidal phases.

5.3 Rare Earth Element (REE) Concentrations during Storm Flow

During period 1 and period 3, total REE concentrations in both springs were lowest (0.10-0.15 ppb). During period 2, with the arrival of storm water, total REE concentrations increase at both springs (up to 1.30 ppb). Total REE concentrations in spring water showed a strong positive correlation with Zr and Fe concentrations (Figure 12). Increased total REE concentrations also appear to be influenced by the intensity of recharge and surface connectivity, with a relatively greater REE increase during the larger June Storm than the May Storm, and a relatively greater REE increase for Tippery Spring than Near Tippery Spring. During pre-storm and matrix-flow conditions, total REE concentrations were consistently low, indicating minor contribution from carbonate matrix dissolution. Furthermore, there was a weaker cerium anomaly at Tippery Spring, which further highlights Tippery Spring's greater conduit-flow influence, but also suggests that a cerium anomaly may be a sensitive indicator of conduit flow mixing with slower matrix flow during storm recovery.

Total REE increased with Zr, indicating REEs are introduced into the aquifer during storm flow sourced from the same areas as the Zr-bearing sediments, namely the high-Zr low-Ca clastic ridge tops feeding into the sinkholes.

Total REE concentrations correlated well with the relative fraction of matrix water and storm water, with increased total REEs occurring with a greater storm water fraction (Figure 13). The lowest REE concentrations (<0.15 ppb) occurred in spring water with the greatest pre-storm

water fraction signature (pre-storm baseflow samples). With the arrival of storm water after rain events, REE concentrations increased with increasing storm water component to the springs, with the greatest REE concentrations (>0.8 ppb) occurring near maximum storm water fraction. Although these relationships generally held true for both springs when the pre-storm water or storm water fractions dominated, the transition from low to high REE concentrations as the slower matrix flow mixed with the faster conduit flow storm water was not smooth. Between storm water fractions of 0.3-0.7, total REE concentrations were highly variable between the maximum and minimum concentrations seen during high matrix-water fraction and high storm-water fraction, respectively. This imperfect transition is likely due to irregular REE mobility from changing pH and redox conditions from mixing water sources after a storm, but could also be the result of recharge source area heterogeneities affecting REE mobility in different source areas.

6. Conclusions

6.1 Storm Response Characteristics of Tippery and Near Tippery Springs

First analyzed for flow characterization by Shuster and White (1971), Tippery Spring and Near Tippery Spring were classified as conduit-flow dominated springs based on their seasonally variable water temperature and chemistry. While being classified as conduit-flow, it was also noted that the springs exhibited distinct behaviors despite their close proximity. Using high-resolution logging and water sampling in response to storms, these springs were re-examined to better define the varying degrees of faster conduit flow and slower flow along with multiple recharge modes for the two springs.

Of the two springs, Tippery Spring exhibited more dominant fast-flow conduit behavior through rapid storm response and recovery of discharge and chemistry, while Near Tippery Spring exhibited a relatively delayed storm response, buffered geochemistry, and drawn-out recovery. These comparative differences between the two springs were maintained during the smaller May 2017 Storm and the larger June 2017 Storm, indicating behaviors intrinsic to the natural recharge and flow characteristic of each spring's recharge area rather than storm intensity or antecedent conditions. Despite the inherent differences, both springs did experience a similar sequence of storm response characteristics marked by the following periods: Period 1) Storm piston pulse, Period 2) Storm water arrival including varying degrees of faster conduit dominant flow and slower matrix dominant flow, and Period 3) Post-storm recovery. The relative timing and duration of these three flow periods were a function of the intrinsic nature of recharge and flow for each spring along with storm intensity. A larger storm produced a greater Period 2 duration, and a stronger surface connection (such as Tippery Spring) had a relatively shorter Period 1 duration and greater Period 2 conduit-flow phase. The nature of these periods, unique to each spring, has important hydrological implications such as water sampling intervals and contaminant storage and transport. A spring with Near Tippery's characteristics with a longer recovery should be sampled longer, while Tippery Spring needs a finer interval to capture different pulses of storm water. Furthermore, constituents associated with sediment transport showed a longer recovery and should be sampled for a longer time to better understand their transport behavior.

6.2 New Tracers for Recharge and Flow Paths

Two natural tracers were applied in new ways for this study: Ca/Zr ratios and REE patterns. Both tracers provided additional information about flow paths and recharge sources as they varied during the storm hydrograph. Stable water isotopes directly indicated the arrival of storm water to the springs while Ca/Zr ratios provided insight into recharge area source and timing. These patterns and results may be shared among other karst systems with allogenic recharge from siliciclastic areas, while karst systems with autogenic recharge may show muted response in these tracers due to greater flow path lengths and more buffered storm recharge behavior.

During pre-storm baseflow, high Ca/Zr ratios reflected water which has dominantly interacted with the carbonate host rock. With the arrival of storm water, Ca/Zr ratios dropped as the previously elevated Ca concentrations from storage became diluted by storm water while Zr concentrations increased from the influx of storm water which had interacted with clastic surface sediments. As a storm water arrival indicator in clastic-ridge-fed Valley and Ridge springs, this relationship made Ca/Zr ratios a useful substitute for stable water isotopes while also providing information on source area. An advantage of the Ca/Zr signature is that Zr analysis is typically provided with other trace elements, whereas stable water isotopes typically require extensive sampling to develop a local meteoric water line and additional analytical techniques.

REE concentrations were lowest (<0.15 ppb) at both springs during baseflow conditions. In response to storm water recharge, REE concentrations increased with the arrival of storm water. REE spidergrams varied throughout different periods of storm response. For these springs, REE patterns during periods of little storm water influence (periods 1 and 3) exhibited negative cerium anomalies which were weak (Tippery Spring) to moderate (Near Tippery Spring). This behavior coincided with the conceptual model of Tippery Spring being inherently more conduit-flow dominated while Near Tippery Spring is inherently more affected by slower flow. During periods of surficial sediment recharge (Period 2) the REE patterns exhibited neutral ($Ce^* = 1$) cerium anomalies, suggesting the storm-recharged sediment was derived from the clastic rocks along the ridges rather than the local carbonate bedrock. Elevated REE concentrations persisting after other parameters recovered to pre-storm levels suggested slower flow paths recharging the two springs which was less apparent with the other parameters.

These results illustrate the sensitivity of REE concentrations and anomalies in karst springs to storm events, recharge areas, and flow paths. Even as other storm flow indicators (e.g. stable water isotopes, TSS, Mg/Ca ratios) may have subsided, elevated REE concentrations and altered cerium anomalies may linger for an extended period of time. As such, the presence of low REE concentrations, along with a pronounced cerium anomaly, may be a good indicator of matrix-affected recharge and storm flow recovery to a spring. Elevated REE concentrations after a storm, along with neutralized cerium anomaly, differentiate between water which has interacted with either the local carbonate matrix or the upland siliciclastics.

This study illustrated the relationships among multiple tracers to understand source waters in different periods of storm hydrographs. REE concentrations, along with other parameters such as stable water isotopes, Mg/Ca and Ca/Zr ratios, provided a more complete understanding of

karst flow and recharge paths, and showed how contrasts between adjacent springs differentiates recharge pathways.

Acknowledgements

The authors would like to acknowledge the National Science Foundation's Hydrologic Sciences Program under award number 1417477. Special thanks to the landowners of the springs who allowed us access and to the journal reviewers for their helpful feedback.

References

Ali, S., Ghosh, N.C., Singh, R., 2010. Rainfall–runoff simulation using a normalized antecedent precipitation index. Hydrol. Sci. J. 55, 266–274. https://doi.org/10.1080/02626660903546175

Bakalowicz, M., 2005. Karst groundwater : a challenge for new resources. Hydrogeol. J. 13, 148–160. https://doi.org/10.1007/s10040-004-0402-9

Berg, T.M., Edmunds, W.E., Geyer, A.R., 1980. Geologic Map of Pennsylvania (2nd ed.), Pennsylvania Geological Survey. Harrisburg, PA.

Berglund, J.L., Toran, L., Herman, E.K., 2018. Using stable isotopes to distinguish sinkhole and diffuse storm infiltration in two adjacent springs, in: NCKRI Symposium 7 15th Sinkhole Conference.

Birk, S., Liedl, R., Sauter, M., 2004. Identification of localised recharge and conduit flow by combined analysis of hydraulic and physico-chemical spring responses (Urenbrunnen, SW-Germany). J. Hydrol. 286, 179–193. https://doi.org/10.1016/j.jhydrol.2003.09.007

Caetano Bicalho, C., Batiot-Guilhe, C., Seidel, J.L., Van Exter, S., Jourde, H., 2012. Geochemical evidence of water source characterization and hydrodynamic responses in a karst aquifer. J. Hydrol. 450–451, 206–218. https://doi.org/10.1016/j.jhydrol.2012.04.059

Desmarais, K., Rojstaczer, S., 2002. Inferring source waters from measurements of carbonate spring response to storms. J. Hydrol. 260, 118–134. https://doi.org/10.1016/S0022-1694(01)00607-2

Doctor, D.H., Alexander, E.C., Kuniansky, E.L., 2005. Interpretation of water chemistry and stable isotope data from a karst aquifer according to flow regimes identified through hydrograph recession analysis. U.S. Geol. Surv. Karst Interes. Gr. Proceedings, Rapid City, South Dakota, Sept. 12-15, 2005 82–92.

Duvert, C., Cendón, D.I., Raiber, M., Seidel, J.L., Cox, M.E., 2015. Seasonal and spatial variations in rare earth elements to identify inter-aquifer linkages and recharge processes in an Australian catchment. Chem. Geol. 396, 83–97. https://doi.org/10.1016/j.chemgeo.2014.12.022

Filippini, M., Squarzoni, G., De Waele, J., Fiorucci, A., Vigna, B., Grillo, B., Riva, A., Rossetti, S., Zini, L., Casagrande, G., Stumpp, C., Gargini, A., 2018. Differentiated spring behavior under changing hydrological conditions in an alpine karst aquifer. J. Hydrol. 556, 572–584. https://doi.org/10.1016/j.jhydrol.2017.11.040

Ford, D., Williams, P., 2007. Karst Hydrogeology, in: Karst Hydrogeology and Geomorphology. John Wiley & Sons Ltd., pp. 103–144. https://doi.org/10.1016/B978-0-08-050762-0.50009-7

Gill, L.W., Babechuk, M.G., Kamber, B.S., McCormack, T., Murphy, C., 2018. Use of trace and rare earth elements to quantify autogenic and allogenic inputs within a lowland karst network. Appl. Geochemistry 90, 101–114. https://doi.org/10.1016/j.apgeochem.2018.01.001

Göb, S., Loges, A., Nolde, N., Bau, M., Jacob, D.E., Markl, G., 2013. Major and trace element compositions (including REE) of mineral, thermal, mine and surface waters in SW Germany and implications for water-rock interaction. Appl. Geochemistry 33, 127–152. https://doi.org/10.1016/j.apgeochem.2013.02.006

Goldscheider, N., 2015. Karst Aquifers—Characterization and Engineering 127–145. https://doi.org/10.1007/978-3-319-12850-4

Goldscheider, N., Meiman, J., Pronk, M., Smart, C., 2008. Tracer tests in karst hydrogeology and speleology. Int. J. Speleol. 37, 27–40. https://doi.org/10.5038/1827-806X.37.1.3

Henderson, P., 1984. Rare Earth Element Geochemistry. Elsevier, Amsterdam.

Herman, E.K., Toran, L., White, W.B., 2009. Quantifying the place of karst aquifers in the groundwater to surface water continuum: A time series analysis study of storm behavior in Pennsylvania water resources. J. Hydrol. 376, 307–317. https://doi.org/10.1016/j.jhydrol.2009.07.043

Hua, G., Yuansheng, D., Lian, Z., Jianghai, Y., Hu, H., 2013. Trace and rare earth elemental geochemistry of carbonate succession in the Middle Gaoyuzhuang Formation, Pingquan Section: Implications for Early Mesoproterozoic ocean redox conditions. J. Palaeogeogr. 2, 209–221. https://doi.org/10.3724/SP.J.1261.2013.00027

Hull, L.C., 1980. Mechanisms controlling the inorganic and isotopic geochemistry of springs in a

carbonate terrane. The Pennsylvania State University.

Ingri, J., Widerlund, A., Land, M., Gustafsson, Ö., Andersson, P., Öhlander, B., 2000. Temporal variations in the fractionation of the rare earth elements in a Boreal river; the role of colloidal particles. Chem. Geol. 166, 23–45. https://doi.org/10.1016/S0009-2541(99)00178-3

Johannesson, K.H., Stetzenbach, K.J., Hodge, V.F., 1997. Rare earth elements as geochemical tracers of regional groundwater mixing. Geochim. Cosmochim. Acta 61, 3605–3618. https://doi.org/10.1016/S0016-7037(97)00177-4

Johannesson, K.H., Zhou, X., Guo, C., Stetzenbach, K.J., Hodge, V.F., 2000. Origin of rare earth element signatures in groundwaters of circumneutral pH from southern Nevada and eastern California, USA. Chem. Geol. 164, 239–257. https://doi.org/10.1016/S0009-2541(99)00152-7

Kresic, N., 1995. Remote sensing of tectonic fabric controlling groundwater flow in Dinaric karst. Remote Sens. Environ. 53, 85–90. https://doi.org/10.1016/0034-4257(95)00042-Y

Lakey, B., Krothe, C., 1996. Stable isotopic variation of storm discharge from a perennial karst spring, Indiana. Water Resour. Res. 32, 721–731.

Larocque, M., Mangin, A., Razack, M., 1998. Contribution of correlation and spectral analyses to the regional study of a large karst aquifer (Charente , France) 205, 217–231.

Leybourne, M.I., Johannesson, K.H., 2008. Rare earth elements (REE) and yttrium in stream waters, stream sediments, and Fe-Mn oxyhydroxides: Fractionation, speciation, and controls over REE + Y patterns in the surface environment. Geochim. Cosmochim. Acta 72, 5962–5983. https://doi.org/10.1016/j.gca.2008.09.022

Luhmann, A.J., Covington, M.D., Peters, A.J., Alexander, S.C., Anger, C.T., Green, J.A., Runkel, A.C., Alexander, E.C., 2011. Classification of Thermal Patterns at Karst Springs and Cave Streams. Ground Water 49, 324–335. https://doi.org/10.1111/j.1745-6584.2010.00737.x

Mangin, A., 1994. Karst hydrogeology, in: Stanford, J., Gibert, J. (Eds.), Groundwater Ecology. Academic Press, pp. 43–67.

Martin, J.B., Kurz, M.J., Khadka, M.B., 2016. Climate control of decadal-scale increases in apparent ages of eogenetic karst spring water. J. Hydrol. 540, 988–1001. https://doi.org/10.1016/j.jhydrol.2016.07.010

Mitrofan, H., Marin, C., Povară, I., 2015. Possible Conduit-Matrix Water Exchange Signatures Outlined at a Karst Spring. Groundwater 53, 113–122. https://doi.org/10.1111/gwat.12292

Möller, P., Dulski, P., Salameh, E., Geyer, S., 2006. Characterization of the sources of thermal spring- and well water in Jordan by rare earth element and yttrium distribution and stable isotopes of H2O. Acta Hydrochim. Hydrobiol. 34, 101–116. https://doi.org/10.1002/aheh.200500614

Noack, C.W., Dzombak, D.A., Karamalidis, A.K., 2014. Rare earth element distributions and trends in natural waters with a focus on groundwater. Environ. Sci. Technol. 48, 4317–4326. https://doi.org/10.1021/es4053895

Padilla, A., Pulido-Bosch, A., Mangin, A., 1994. Relative importance of baseflow and quickflow from hydrographs of karst spring. Groundwater 32, 267–277.

Pinault, J., Plagnes, V., Aquilina, L., 2001. Inverse modeling of the hydrological and the hydrochemical behavior of hydrosystems : Characterization of karst system functioning. Water Resour. Res. 37, 2191–2204.

Playà, E., Cendón, D.I., Travé, A., Chivas, A.R., García, A., 2007. Non-marine evaporites with both inherited marine and continental signatures: The Gulf of Carpentaria, Australia, at ~ 70 ka. Sediment. Geol. 201, 267–285. https://doi.org/10.1016/j.sedgeo.2007.05.010

Pourmand, A., Dauphas, N., Ireland, T.J., 2012. A novel extraction chromatography and MC-ICP-MS technique for rapid analysis of REE, Sc and Y: Revising CI-chondrite and Post-Archean Australian Shale (PAAS) abundances. Chem. Geol. 291, 38–54. https://doi.org/10.1016/j.chemgeo.2011.08.011

Pourret, O., Gruau, G., Dia, A., Davranche, M., Molénat, J., 2010. Colloidal control on the distribution of rare earth elements in shallow groundwaters. Aquat. Geochemistry 16, 31–59. https://doi.org/10.1007/s10498-009-9069-0

Ravbar, N., Engelhardt, I., Goldscheider, N., 2011. Anomalous behaviour of specific electrical conductivity at a karst spring induced by variable catchment boundaries: The case of the Podstenjšek spring, Slovenia. Hydrol. Process. 25, 2130–2140. https://doi.org/10.1002/hyp.7966

Ryan, M., Meiman, J., 1996. An examination of short-term variation sin water quality at a karst spring in Kentucky. Ground Water 34, 23–30.

Scanlon, B.R., Thrailkill, J., 1987. Chemical similarities among physically distinct spring types in a karst terrain. J. Hydrol. 89, 259–279.

Schwartz, B.F., Schreiber, M.E., 2009. Quantifying potential recharge in mantled sinkholes using ERT. Ground Water 47, 370–381. https://doi.org/10.1111/j.1745-6584.2008.00505.x

Schwarz, K., Barth, J.A.C., Postigo-Rebollo, C., Grathwohl, P., 2009. Mixing and transport of water in a karst catchment: A case study from precipitation via seepage to the spring. Hydrol. Earth Syst. Sci. 13, 285–292. https://doi.org/10.5194/hess-13-285-2009

Shuster, E.T., White, W.B., 1971. Seasonal fluctuations in the chemistry of lime-stone springs: A possible means for characterizing carbonate aquifers. J. Hydrol. 14, 93–128. https://doi.org/10.1016/0022-1694(71)90001-1

Tang, J., Johannesson, K.H., 2006. Controls on the geochemistry of rare earth elements along a groundwater flow path in the Carrizo Sand aquifer, Texas, USA. Chem. Geol. 225, 156–171. https://doi.org/10.1016/j.patcog.2005.08.006

Toran, L., Herman, E.K., Berglund, J.L., 2018. Advances in Monitoring to Understand Flow Paths in Karst: Comparison of Historic and Recent Data from the Valley and Ridge of Pennsylvania, in: The Handbook of Environmental Chemistry. Springer, pp. 65–89.

Toran, L., Reisch, C.E., 2013. Using stormwater hysteresis to characterize karst spring discharge. Groundwater 51, 575–587. https://doi.org/10.1111/j.1745-6584.2012.00984.x

Tweed, S.O., Weaver, T.R., Cartwright, I., Schaefer, B., 2006. Behavior of rare earth elements in groundwater during flow and mixing in fractured rock aquifers: An example from the Dandenong Ranges, southeast Australia. Chem. Geol. 234, 291–307. https://doi.org/10.1016/j.chemgeo.2006.05.006

White, W.B., 2002. Karst hydrology: Recent developments and open questions. Eng. Geol. 65, 85–105. https://doi.org/10.1016/S0013-7952(01)00116-8

White, W.M., 2015. Isotope Geochemistry, 1st ed. Wiley Works, West Sussex.

Willis, S.S., Johannesson, K.H., 2011. Controls on the geochemistry of rare earth elements in sediments and groundwaters of the Aquia aquifer, Maryland, USA. Chem. Geol. 285, 32–49. https://doi.org/10.1016/j.chemgeo.2011.02.020

Winston, W.E., Criss, R.E., 2004. Dynamic hydrologic and geochemical response in a perennial karst spring. Water Resour. Res. 40, 1–11. https://doi.org/10.1029/2004WR003054

Zhao, M., Hu, Y., Zeng, C., Liu, Z., Yang, R., Chen, B., 2018. Effects of land cover on variations in stable hydrogen and oxygen isotopes in karst groundwater: A comparative study of three karst catchments in Guizhou Province, Southwest China. J. Hydrol. 565, 374–

385. https://doi.org/10.1016/j.jhydrol.2018.08.037

Zhou, H., Greig, A., Tang, J., You, C.F., Yuan, D., Tong, X., Huang, Y., 2012. Rare earth element patterns in a Chinese stalagmite controlled by sources and scavenging from karst groundwater. Geochim. Cosmochim. Acta 83, 1–18. https://doi.org/10.1016/j.gca.2011.12.027

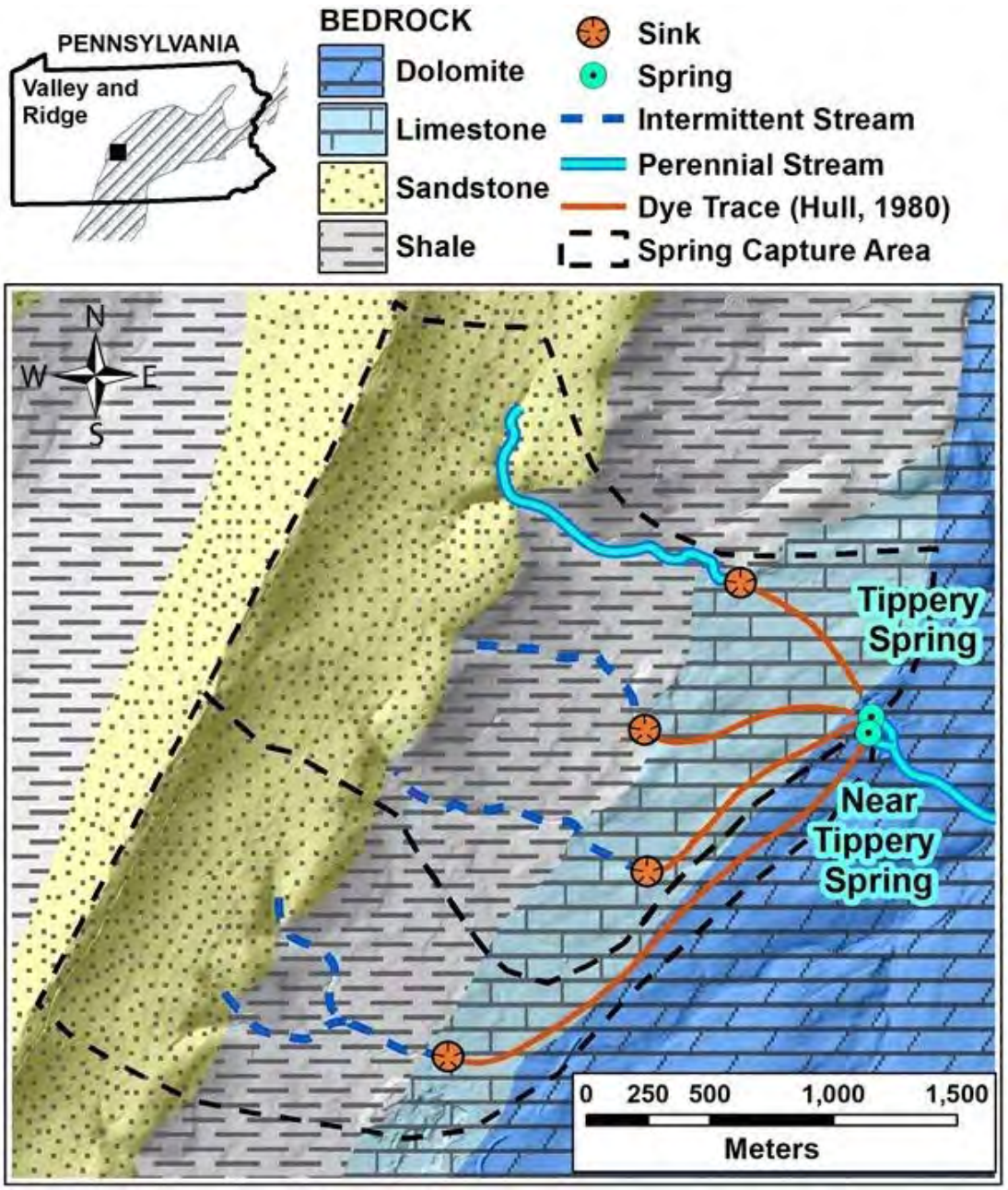

Figure 1. Map of study area for Tippery Spring and Near Tippery Spring.

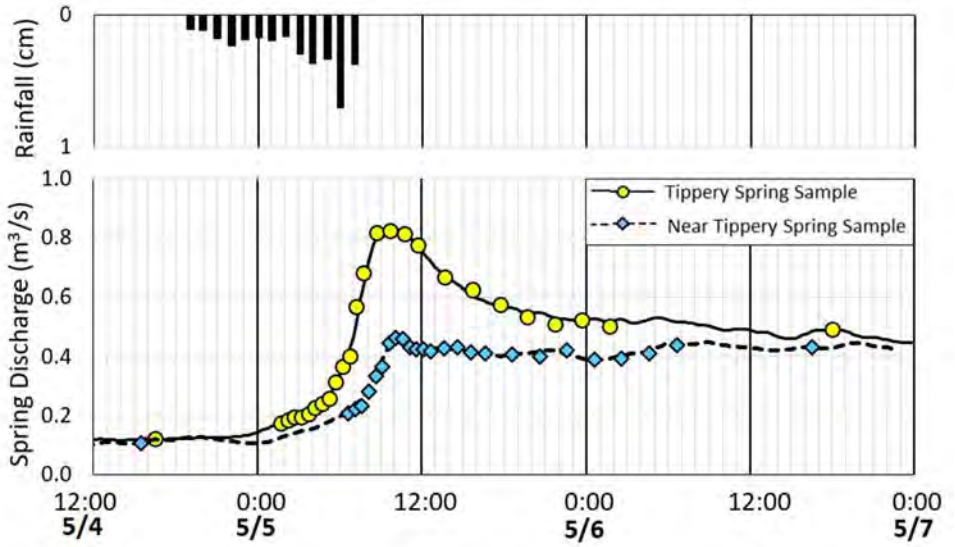

Figure 2. May 2017 Storm rainfall, spring hydrograph, and sample times for Tippery Spring and Near Tippery Spring. Spring discharge is calculated from 15-minute interval water level readings at each spring's weir. Rainfall was calculated from hourly rain gauge totals.

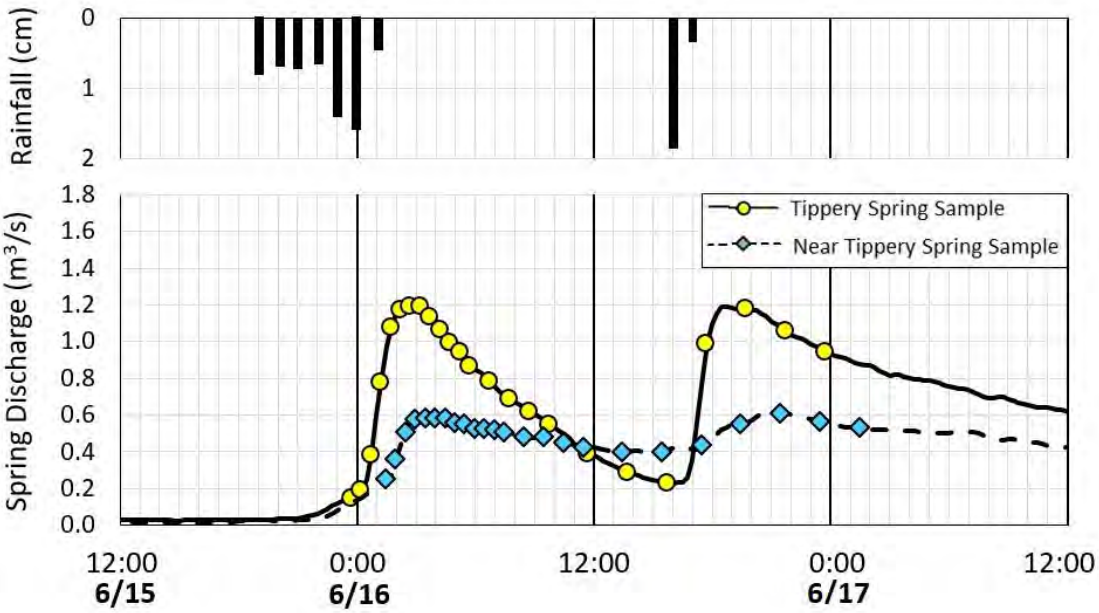

Figure 3. June 2017 Storm rainfall, spring discharge, and sample times for Tippery Spring and Near Tippery Spring. Spring discharge is calculated from 15-minute interval water level readings at each spring's weir. Rainfall was calculated from hourly rain gauge totals.

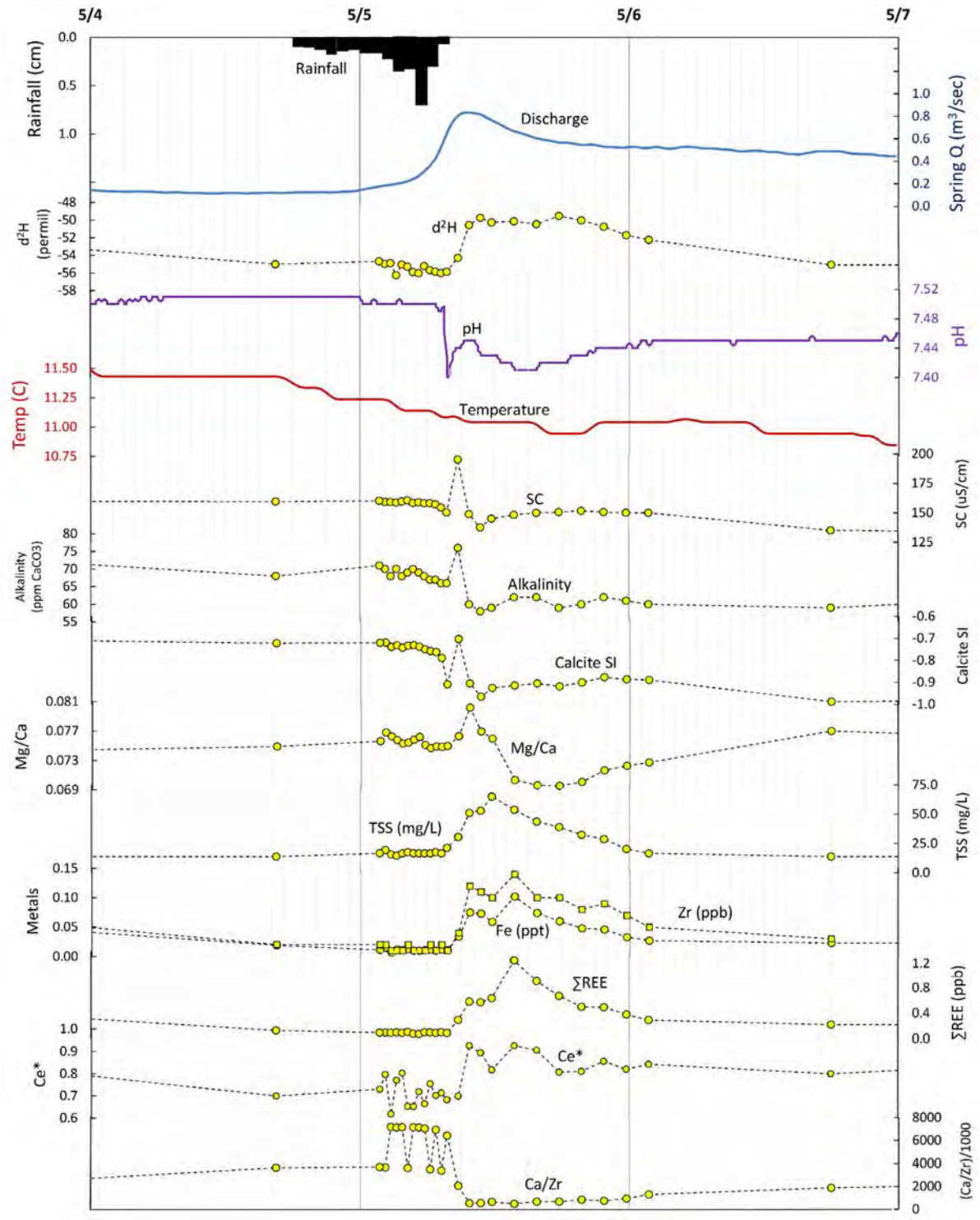

Figure 4. Tippery Spring May 2017 Storm results. Solid plot lines represent logger data. Dashed lines connect water sample point values. Major vertical grid at 24 hour interval, minor vertical grid at 1 hour interval.

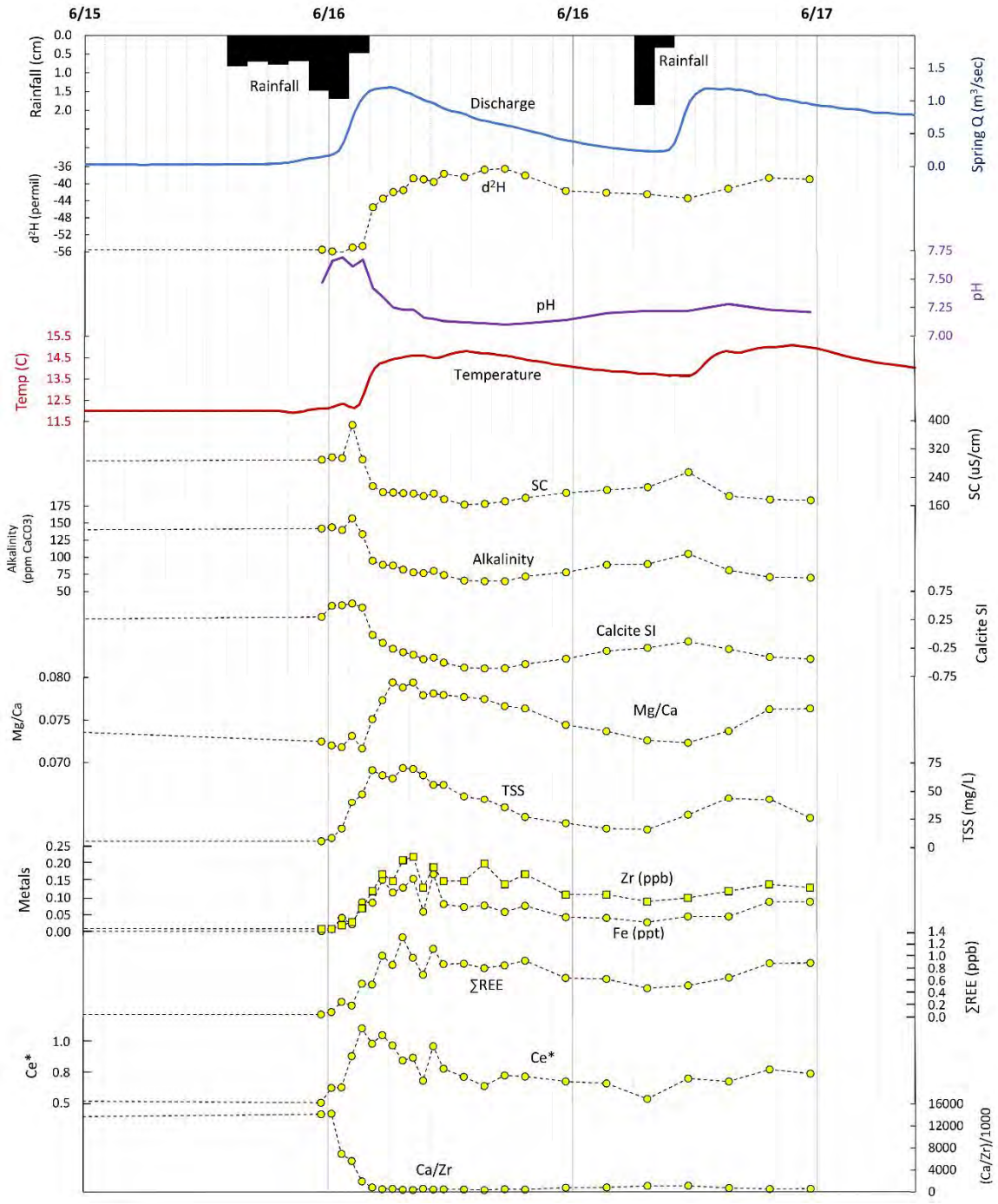

Figure 5. Tippery Spring June 2017 Storm results. Solid plot lines represent logger data. Dashed lines connect water sample point values. Major vertical grid at 12 hour interval, minor vertical grid at 1 hour interval. The data were plotted to center the storm and show recovery even though the pre-storm grab sample is off the scale and a post storm grab sample was not available.

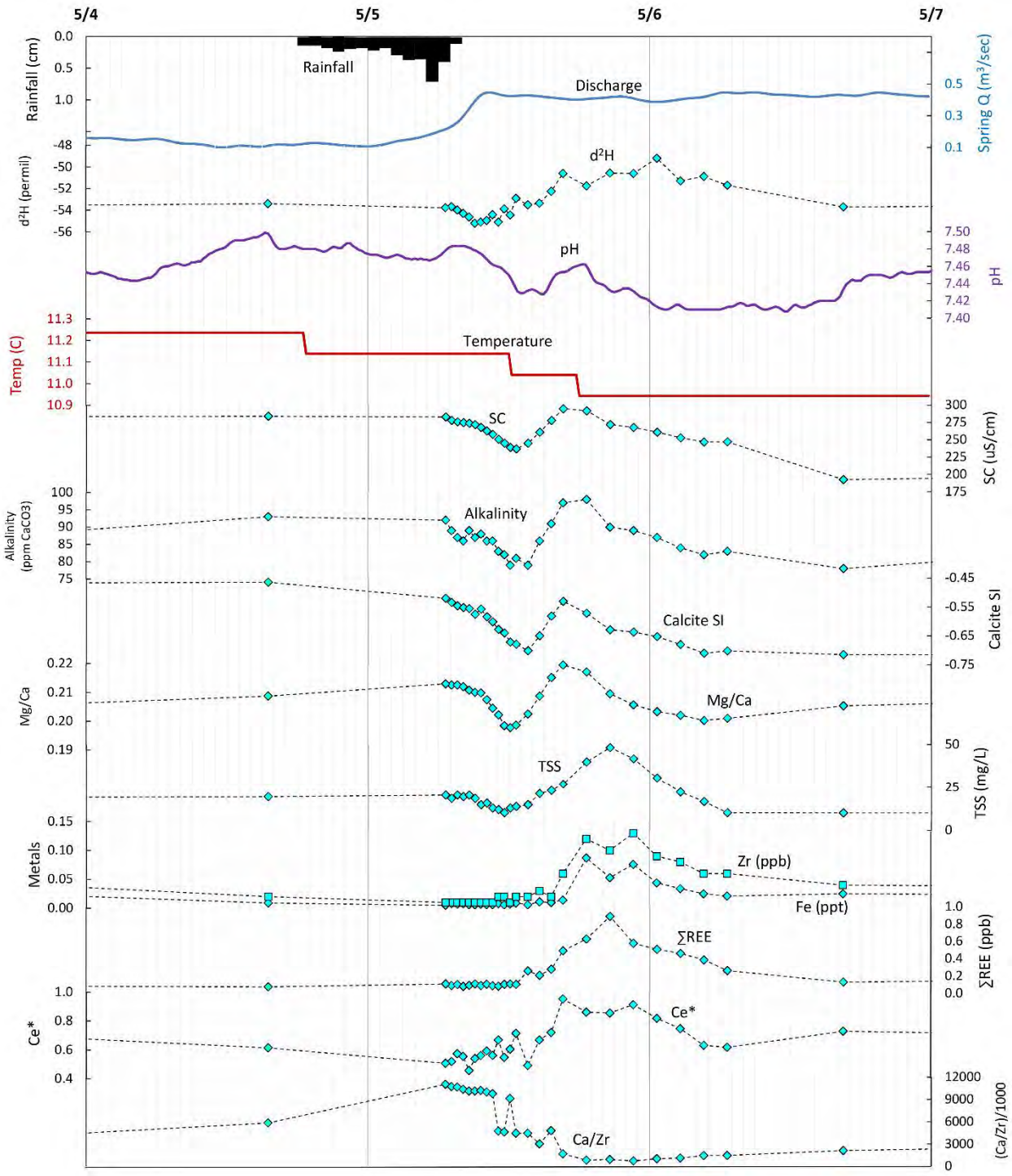

Figure 6. Near Tippery Spring May 2017 Storm results. Solid plot lines represent logger data. Dashed lines connect water sample point values. Major vertical grid at 24 hour interval, minor vertical grid at 1 hour interval.

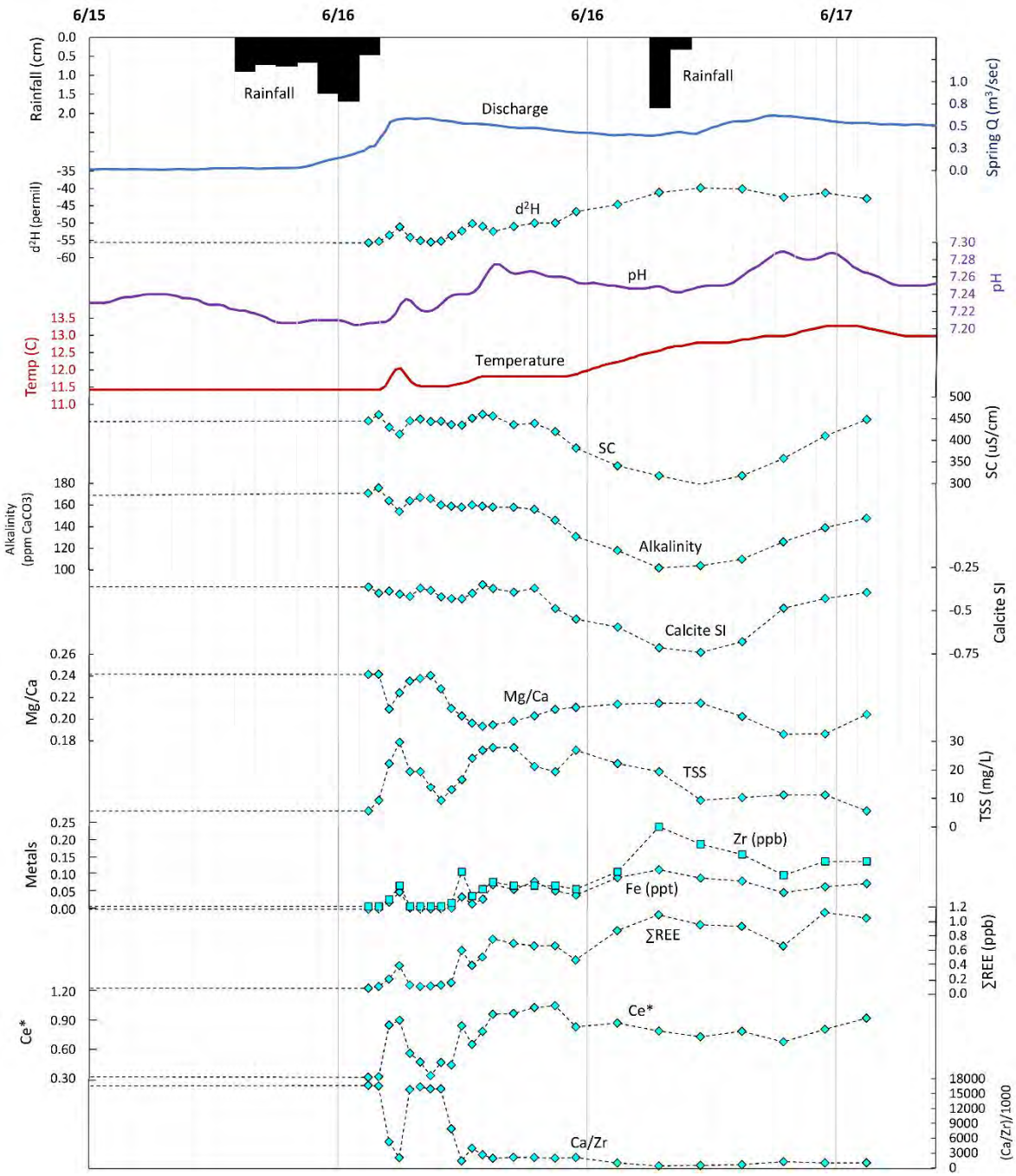

Figure 7. Near Tippery Spring June 2017 Storm results. Solid plot lines represent logger data. Dashed lines connect water sample point values. Major vertical grid at 12 hour interval, minor vertical grid at 1 hour interval. The data were plotted to center the storm and show recovery even though the pre-storm grab sample is off the scale and a post storm grab sample was not available.

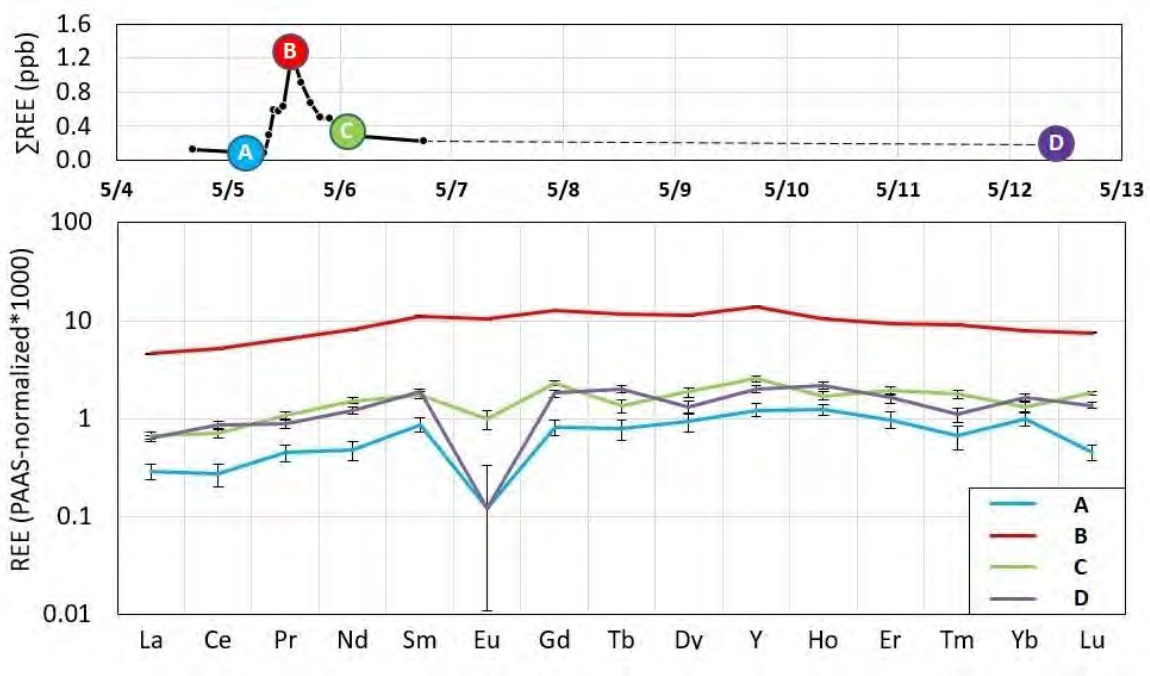

Figure 8. PAAS-normalized REE spidergrams for Tippery Spring during the May 2017 Storm during select storm response sample times: A) Pre-storm, B) Peak REE Concentration, C) REE Concentration Falling Limb, and D) Post-storm.

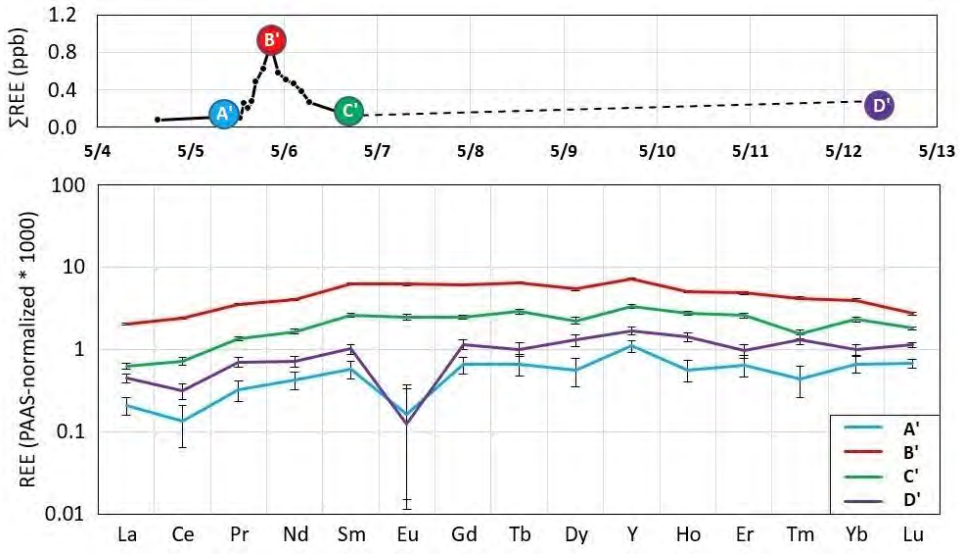

Figure 9. PAAS-normalized REE spidergrams for Near Tippery Spring during the May 2017 Storm at select periods of storm response sample times: A') Pre-storm, B') Peak REE Concentration, C') REE Concentration Falling Limb, and D') Post-storm.

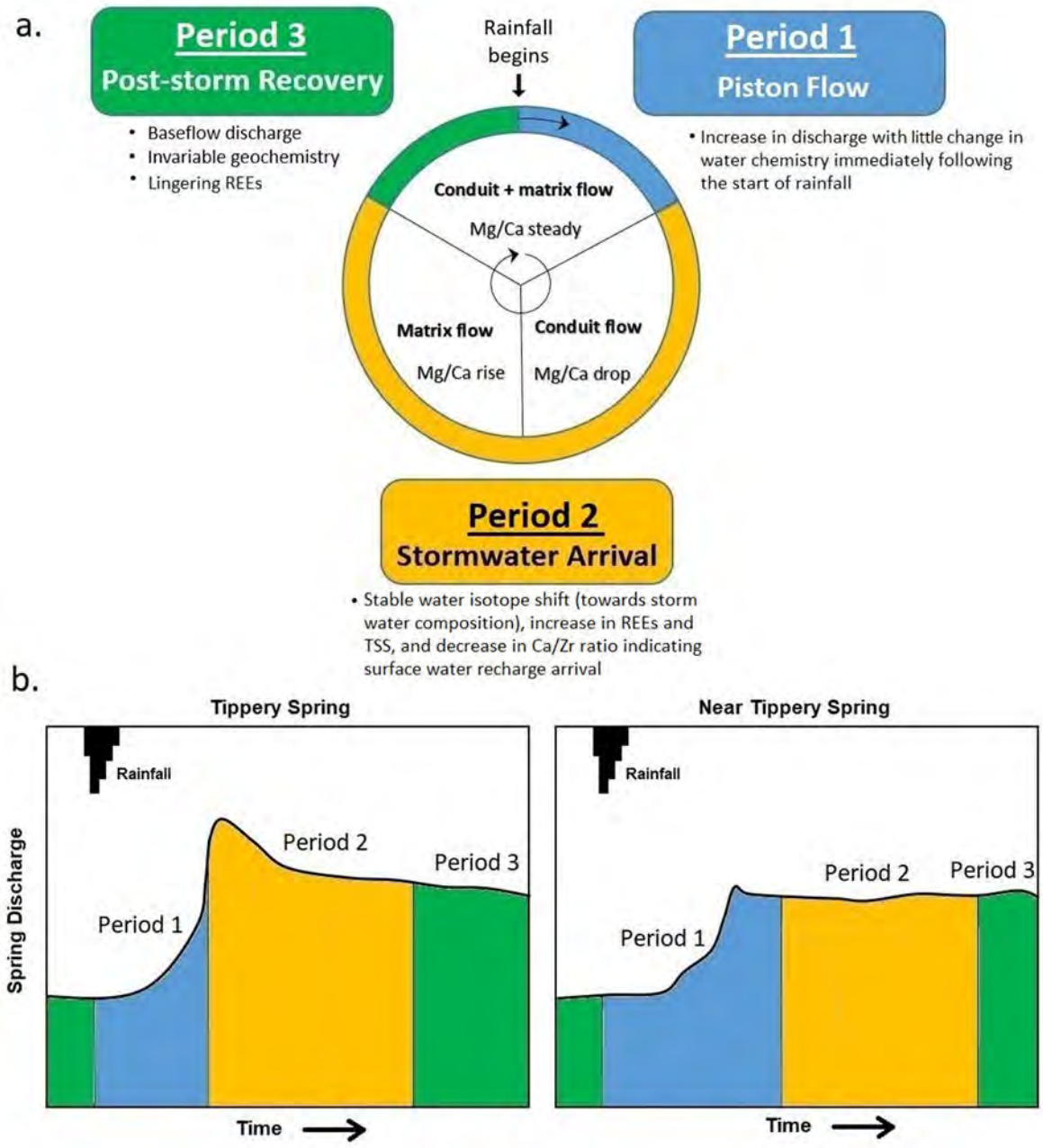

Figure 10. a) Storm response cycle for Tippery Spring and Near Tippery Spring consisting of three periods with similar discharge and geochemical responses; Period 1) Storm Pressure Pulse, Period 2) Storm water Arrival, and Period 3) Post-storm Recovery. b) Idealized hydrographs with timing of three periods for each spring following the same rain event. The arrival timing and duration of each Period, along with the relative abundance of faster conduit-flow vs. slower matrix-flow, is unique to each spring.

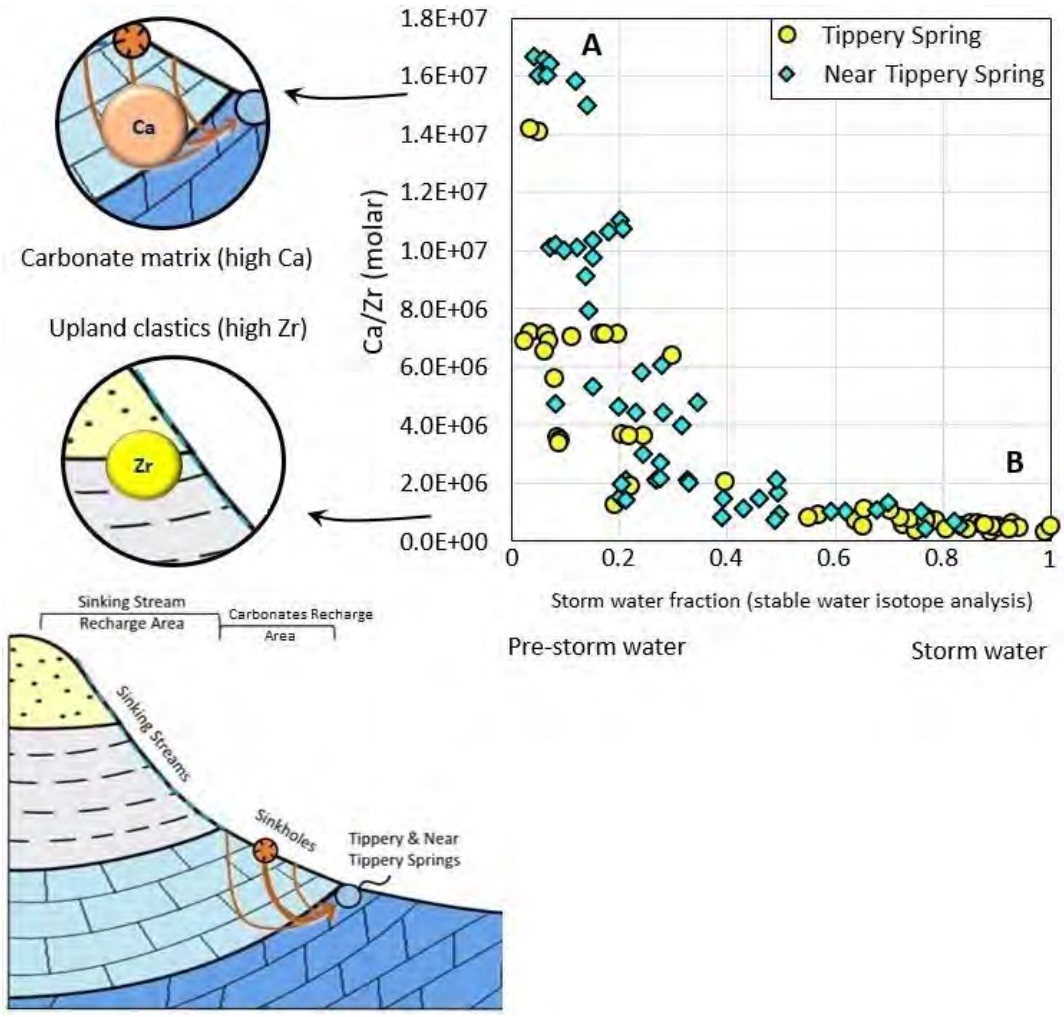

Figure 11. Relationship between storm water component and Ca/Zr ratio in spring water as an indicator of recharge area. During low storm water flow component, a high Ca/Zr ratio suggests a high carbonate matrix-water component. During high storm water flow component, a low Ca/Zr ratio suggests recharging water having interacted with Zr-rich and Ca-poor clastic sediments from upland clastic ridges and transporting Zr and Ca in both dissolved and colloidal phases (<0.45µm).

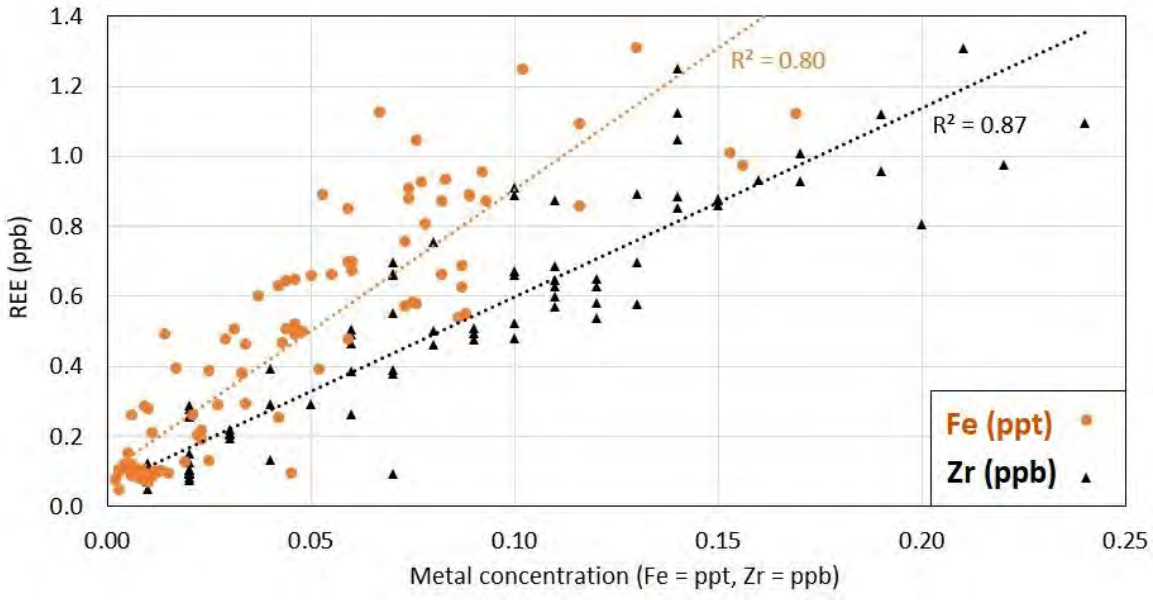

Figure 12. Relationship between total REE concentration and metals such as iron (Fe) and zirconium (Zr) in all spring water samples at Tippery Spring and Near Tippery Spring during the May Storm and June Storm.

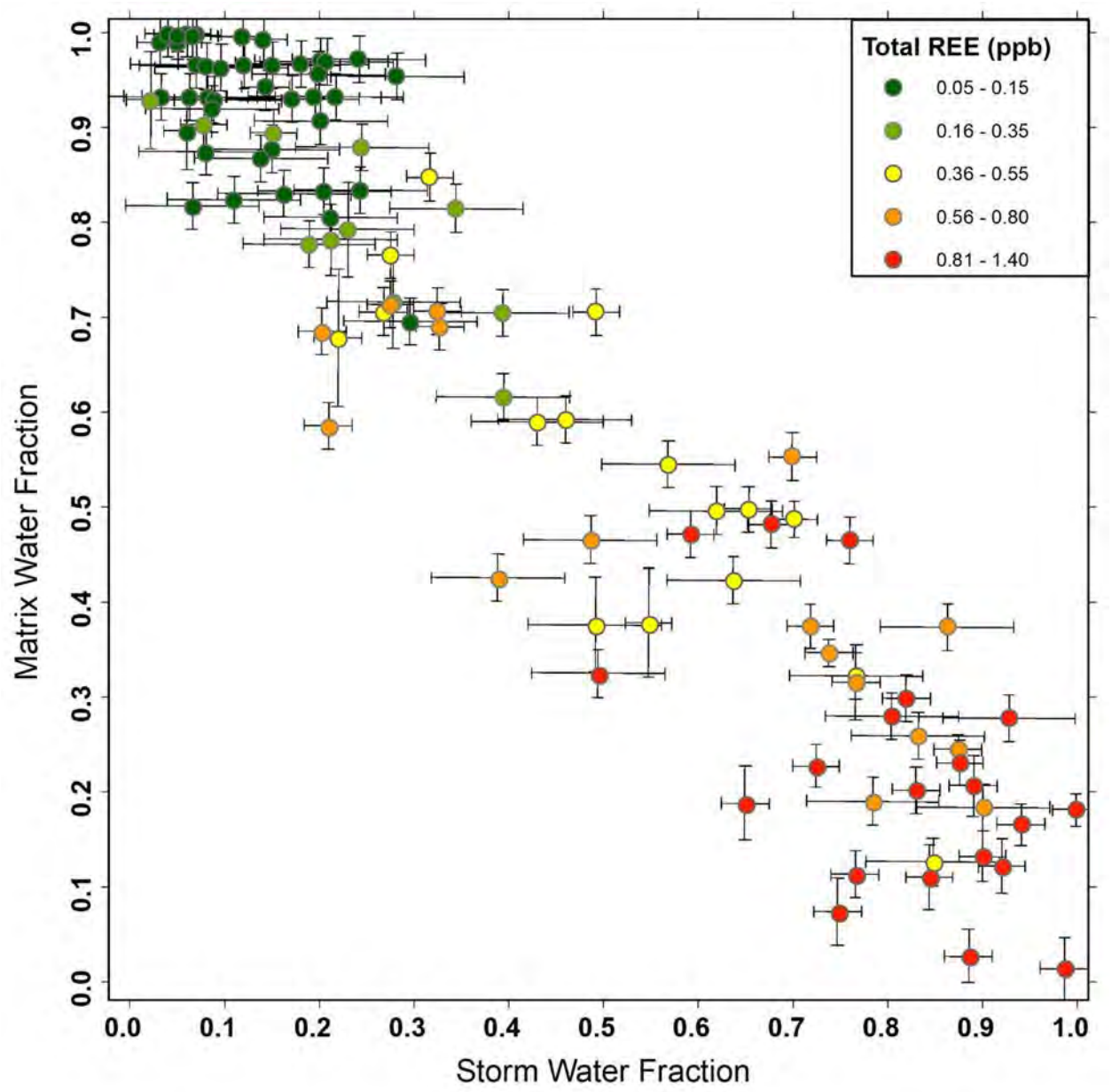

Figure 13. Total REE concentrations on a mixing line between high stored water fraction and high storm water fraction based on hydrograph analysis of stable water isotopes and Ca/Zr ratios. The lowest total REE concentrations occur during high stored water fraction while the highest total REE concentrations occur during a high storm water fraction.